HHS Public Access

Author manuscript

J Am Soc Echocardiogr. Author manuscript; available in PMC 2019 March 15.

Published in final edited form as:

J Am Soc Echocardiogr. 2015 June ; 28(6): 718–26.e2. doi:10.1016/j.echo.2015.02.002.

REAL-TIME CONTRAST ULTRASOUND MUSCLE PERFUSION IMAGING WITH INTERMEDIATE-POWER IMAGING COUPLED WITH ACOUSTICALLY-DURABLE MICROBUBBLES

Sang-Hoon Seol, M.D.,
Knight Cardiovascular Institute, Oregon Health & Science University, Portland, Oregon and the Division of Cardiology, Haeundae Paik Hospital, Inje University College of Medicine, Busan, Korea

Brian P. Davidson, M.D.,
Knight Cardiovascular Institute, Oregon Health & Science University, Portland, Oregon and the Division of Cardiology, Haeundae Paik Hospital, Inje University College of Medicine, Busan, Korea

J. Todd Belcik, B.S., R.C.S, R.D.C.S,
Knight Cardiovascular Institute, Oregon Health & Science University, Portland, Oregon and the Division of Cardiology, Haeundae Paik Hospital, Inje University College of Medicine, Busan, Korea

Brian H. Mott, M.D.,
Knight Cardiovascular Institute, Oregon Health & Science University, Portland, Oregon and the Division of Cardiology, Haeundae Paik Hospital, Inje University College of Medicine, Busan, Korea

Reid M. Goodman,
Knight Cardiovascular Institute, Oregon Health & Science University, Portland, Oregon and the Division of Cardiology, Haeundae Paik Hospital, Inje University College of Medicine, Busan, Korea

Azzdine Ammi, Ph.D., and
Knight Cardiovascular Institute, Oregon Health & Science University, Portland, Oregon and the Division of Cardiology, Haeundae Paik Hospital, Inje University College of Medicine, Busan, Korea

Jonathan R. Lindner, M.D.

Address correspondence to: Jonathan R. Lindner, MD, Cardiovascular Division, UHN-62, Oregon Health & Science University, 3181, SW Sam Jackson Park Rd., Portland, OR 97239, Tel. (503) 494-8750, Fax. (503) 494-8550, linderj@ohsu.edu.

DISCLOSURES

Sonazoid was for investigation further to a research agreement with GE Healthcare

Knight Cardiovascular Institute, Oregon Health & Science University, Portland, Oregon and the Division of Cardiology, Haeundae Paik Hospital, Inje University College of Medicine, Busan, Korea

Abstract

Background: There is growing interest in limb contrast-enhanced ultrasound (CEU) perfusion imaging for the evaluation of peripheral artery disease. Because of low resting microvascular blood flow in skeletal muscle, signal enhancement during limb CEU is prohibitively low for real-time imaging. We hypothesized that this obstacle can be overcome by intermediate rather than low-power CEU when performed with an acoustically-resilient microbubble agent.

Methods: Viscoelastic properties of Definity and Sonazoid were assessed by measuring bulk modulus during incremental increases in ambient pressure to 200 mm Hg. Comparison of in vivo microbubble destruction and signal enhancement at a mechanical index (MI) of 0.1 to 0.4 was performed by sequential reduction in pulsing interval (PI) from 10 to 0.05 s during limb CEU at 7 MHz in mice and 1.8 MHz in dogs. Destruction was also assessed by broad-band signal generation during passive cavitation detection. Real-time CEU perfusion imaging with destruction-replenishment was then performed at 1.8 MHz in dogs using MI of 0.1, 0.2 or 0.3.

Results: Sonazoid had a higher bulk modulus than Definity (66±12 vs 29±2 kPa, p=0.02) and exhibited less inertial cavitation (destruction) at an MI ≥0.2. On in vivo CEU, maximal signal intensity increased incrementally with MI for both agents, and was equivalent between agents except at MI 0.1 (60% and 85% lower for Sonazoid at 7 and 1.8 MHz, respectively; p<0.05). However, on progressive shortening of the PI, Definity was nearly completely destroyed at MI ≥0.2 at 1.8 and 7 MHz, whereas Sonazoid was destroyed only at 1.8 MHz at MI ≥0.3. As a result, real-time CEU perfusion imaging demonstrated approximately >4-fold greater enhancement for Sonazoid at an MI of 0.3 to 0.4.

Conclusions: Robust signal enhancement during real-time CEU perfusion imaging of the limb is possible when using intermediate-power imaging coupled with a durable microbubble contrast agent.

In patients with suspected coronary artery disease, myocardial perfusion imaging is routinely used to quantify ischemia at rest or during stress. For peripheral artery disease (PAD) there is no widely-accepted method for evaluating limb perfusion. Recent studies suggest that contrast-enhanced ultrasound (CEU) perfusion imaging provides valuable information on PAD disease severity beyond that provided by standard-of-care evaluation.[1–3] However, signal enhancement during limb CEU is relatively low because of low skeletal muscle blood flow (0.05–0.3 ml/min/g) and low functional microvascular blood volume, approximately 50% of that in the myocardium.[4,5] As a result, conventional perfusion imaging with destruction-replenishment analysis during low-power (mechanical index [MI] <0.2) real-time imaging is not feasible even with state-of-the-art multipulse algorithms that maximize microbubble signal relative to tissue. Instead, replenishment kinetics in the limb has been performed with highpower (MI >0.8) “destructive” intermittent imaging which increases signal intensity but is more time-consuming and technically challenging because of the need to maintain the same imaging plane during leg exercise and at the long pulsing intervals needed to reach plateau intensity in skeletal muscle.[1,6] An alternative approach has

been to use transit rate analysis with low-power imaging and intravenous bolus injections.[2,3,7]. This approach produces high microbubble blood concentrations, yet signal enhancement still remains low (<8 dB).

The ultrasound signal intensity from microbubbles achieved during stable cavitation (non-destructive non-linear oscillation) increases with the acoustic pressure applied.[8] During real-time imaging, there is a practical limit to increasing the power because of microbubble destruction, or inertial cavitation, which in the diagnostic frequency range of clinical scanners occurs at an MI >0.2. We hypothesized that real-time imaging with *intermediate* power (MI 0.2 to 0.4) produces high signal intensity during limb CEU perfusion imaging when used in conjunction with acoustically "durable" microbubbles capable of undergoing stable cavitation without destruction at an MI >0.2. We evaluated two microbubble agents used in humans that vary in their acoustic lability due to composition-related differences in viscoelastic damping.[9] To test our hypothesis we: (*a*) measured microbubble pressure lability *in vitro* and *in vivo*, (*b*) analyzed microbubble acoustic amplitude-frequency response to differentiate stable from inertial cavitation, and (*c*) assessed *in vivo* ultrasound signal generation and performed *in vivo* CEU limb perfusion imaging with a range of acoustic pressures.

METHODS

Animals

The study was approved by the Animal Care and Use Committee at Oregon Health & Science University. For murine imaging, we studied 14 wild-type C57Bl/6 mice age 8–12 weeks. Mice were anesthetized with inhaled isoflurane (1.0–1.5%) and a catheter was placed in a jugular vein for administration of microbubbles. For canine imaging, we studied 10 dogs (25 to 31 kg) that were anesthetized with intravenous pentobarbital sodium and placed on a positive pressure ventilator. A cannula was placed in the femoral vein for microbubble administration.

Microbubbles

Two microbubble agents were studied that differ in terms of gas and shell composition: (*a*) Definity which is composed of octafluoropropane gas stabilized by pegylated and non-pegylated dipalmitoyl phospholipids; and (*b*) Sonazoid which is composed of decafluorobutane stabilized primarily by hydrogenated egg phosphatidylserine. The latter agent has been shown to be more resilient and less susceptible to ultrasound-mediated destruction in vitro.[9] Microbubble concentration was measured by electrozone sensing (Multisizer III, Beckman Coulter, Brea, CA).

Microbubble Bulk Modulus

Bulk modulus measured from the relationship between ambient constant pressure and microbubble diameter was used to evaluate compressibility. A syringe containing microbubble suspensions was connected to cellulose tubing with an internal diameter of 200 μm which was placed in the focal plane of a microscope (Axioskop2-FS, Carl Zeiss, Inc., Thornwood, NY) with a water immersion objective (×63/1.3 N.A.). A side port of the

system contained a calibrated micromanometer pressure transducer (SPR–671; Millar Instruments, Inc., Houston, TX). The distal end of the tubing was then clamped and the plunger was advanced by a syringe pump to increase system pressure (P) by approximately by 50 mm Hg increments up to 200 mm Hg for Definity and 300 mm Hg for Sonazoid. Microscope images of microbubbles in the cellulose tubing at each pressure were acquired and microbubble volumes (V) were calculated using diameter measurements assuming spherical geometry. Bulk modulus (K) for a 200 mm Hg pressure change was calculated assuming isotropic conditions and no significant change in wall thickness by: $P/(\Delta V/V_0)$. Measurements were made only for microbubbles with baseline diameters of 3.0–5.0 μm since baseline size independently influences K.[10]

In vivo Acoustic Lability and Skeletal Muscle Signal Enhancement

In order to expand applicability of our results to clinical and pre-clinical settings, *in vivo* experiments were performed using two separate ultrasound systems performing at either high or low diagnostic frequency. High-frequency CEU was performed with a linear-array transducer (Sequoia 512, Siemens Medical Systems, Mountain View, CA) at a frequency of 7 MHz and a dynamic range of 55 dB. The proximal hindlimb adductor muscles of mice were imaged in short-axis. The non-linear fundamental signal component for microbubbles was detected using multipulse phase-inversion and amplitude-modulation imaging. For low MI imaging, the proximal hindlimb adductor muscle group of dogs (n=6) was imaged at 1.8 MHz using broadband amplitude modulation imaging with medium line-density (iE33, Philips Ultrasound, Andover, MA). Imaging in the mice and dogs was performed at a MI of 0.1, 0.2, 0.3 and 0.4, and for each MI gain settings were optimized to a level just below that which showed tissue speckle on pre-contrast imaging. In mice Definity (n=6) or Sonazoid (n=8) was infused at 1×10^7 min^{-1}. In dogs (n=6) microbubbles were infused at 2×10^8 min^{-1} with a latent period of 15 min between agents, the order of which was randomized. Images were obtained using PIs that were progressively shortened from 10 s to 50 ms to assess: (*a*) acoustic lability, defined by the progressive decline in signal enhancement with shorter PI, and (*b*) maximal signal enhancement which was measured at a PI of 10 s which provides sufficient time for complete ultrasound sector volume replenishment in non-ischemic mice and dogs.[11,12]

CEU Perfusion Imaging

Real-time CEU perfusion imaging of the proximal hindlimb in dogs (n=4) was performed using destruction-replenishment analysis and microbubble infusion rates and imaging settings described above. Perfusion imaging was also performed in mice (n=3) with the separate purpose of evaluating Sonazoid signal time-intensity data during real-time imaging (MI 0.2 and 0.4) to that during intermittent high-power (MI 1.0) imaging. Once steady state concentration of microbubbles was achieved, microbubbles within the ultrasound sector volume were destroyed with a high-power (MI >0.9) 5-frame pulse sequence. Real-time microbubble replenishment was assessed at a PI of 0.5 seconds which was deemed to be the longest interval that still would provide a sufficient number of frames to reconstruct a time-intensity plot. For the high-MI murine protocols, the PI was increased from 0.5 to 15 seconds. Background-subtracted intensity was measured using the immediate post-destruction frame as background and time-intensity data were fit to the function:

$$y = A\left(1 - e^{-\beta t}\right)$$

where y is intensity at time t, A is the plateau intensity, and the rate constant β represents the microvascular flux rate.[13,14]

Microbubble Cavitation Response

Microbubble cavitation during ultrasound exposure (1.8 MHz) at an MI of 0.1 to 0.4 was assessed by passive cavitation detection (PCD). A spherically focused broadband (10 KHz to 20 MHz) hydrophone (Y-107, Sonic Concepts, Inc., WA) with a focal depth of 20 mm and a focal width of 0.4 mm was confocally positioned with the ultrasound transducer at a 60° relative angle to receive signals from a flow phantom containing microbubbles. Received signals were digitized (100 MHz) and saved in a 4-channel oscilloscope (Waverunner, Teledyne LeCroy, Chestnut Ridge, NY) using sequence mode. Data analysis was performed with the Matlab (MathWorks, Natick, MA) using data averaged over the entire 20 min exposure period.

Ultrasound Pressure Measurement

Acoustic pressure measurement at each MI for both high- and low-frequency transducers was determined with a polyvinylidene fluoride needle hydrophone (HPM075/1, Precision Acoustics Ltd, Dorchester, Dorset, UK). During calibration, hydrophones were mounted on a computer controlled three-axis translation system (Velmex Inc., Bloomfield, NY, USA) with 2.5 μm precision.

Statistical Analysis

Differences between the two microbubble agents for any given condition was made using unpaired Student's *t*-tests (two-sided). Differences in values according to power were made using one-way ANOVA and post-hoc differences between groups was made with a Tukey test for multiple comparisons. Linear associations were analyzed using regression analysis and Pearson's product-moment correlation; non-linear associations were measured by regression analysis with least-squares fit. Differences in the slope or rate constants were evaluated using ANCOVA analysis of co-variance. Differences were considered significant at $p<0.05$.

RESULTS

Microbubble Compressibility

The mean diameter of microbubbles used for measurement of bulk modulus was similar for Definity and Sonazoid (4.5±0.2 vs 4.4±0.1 μm, p=0.62). With incremental increases in stable ambient pressure, microbubble diameter and microbubble volume progressively decreased for both Definity and Sonazoid (Figure 1). The degree to which size decreased with increasing pressure was greater for Definity than for Sonazoid (ANCOVA $p<0.001$ for both pressure-diameter and pressure-volume relationships). Microbubble bulk modulus measured assuming isotropic conditions and constant wall thickness was greater for

Sonazoid than for Definity (Figure 1D) indicating lower compressibility from differences in viscoelastic properties.

In vivo Acoustic Lability and Signal Intensity

Acoustic destruction of microbubbles *in vivo* was evaluated by the decline in video intensity produced by shortening of the ultrasound PI during a continuous infusion of microbubbles. The peak negative acoustic pressure for the high- and low-frequency transducers for each MI setting are shown in Table 1. The mean diameter for the two microbubble agents was similar, although Sonazoid possessed a narrower size distribution (Supplement Figure A). CEU with variable PIs was performed during high-frequency (7 MHz) contrast-specific imaging of the mouse hindlimb to evaluated signal enhancement and the degree of microbubble destruction. Data are displayed in Figure 2 which shows the full linear range of PIs, and also in Figure 3 which uses an abbreviated linear range of PI's (Figure 3A and3B) and a logcompressed scale (Figure 3C and3D) in order to better appreciate destruction at shorter PIs. With this agent microbubble destruction was seen at MIs of 0.2 and higher, with nearly complete destruction of agent at MI of 0.3 and 0.4 evidenced by nearly complete absence of microbubble signal at the shortest PI. For Sonazoid, signal enhancement was very low at an MI of 0.1 but again intensity increased with MI. Signal intensity did not change with shortening of the PI, indicating very little destruction at 7 MHz even at an MI of 0.4. Examples of CEU images from murine experiments are provided in Supplemental Figure B.

Data formatted in a similar fashion for low frequency (1.8 MHz) contrast-specific imaging of the canine hindlimb are illustrated in Figure 4 and 5. Once again, signal enhancement at long PI for both Definity and Sonazoid tended to increase with MI. Complete destruction of Definity was seen at all MIs of 0.2 and higher, indicated by nearly complete absence of signal at the shortest PIs. For Sonazoid there was evidence for destruction of Sonazoid at MIs of 0.2 and higher unlike the situation seen for high frequency imaging. However, Sonazoid was still more resistant to destruction than Definity during low-frequency imaging, evidenced by greater ($p<0.01$) signal enhancement for Sonazoid at PIs of 0.5 to 1 s when imaging at each MI ≥0.2, and incomplete elimination of signal for Sonazoid at the shortest PI of 50 ms.

In order to quantify maximal signal enhancement at each MI, mean background-subtracted signal at the longest PI of 10 s was compared for the two agents during high- and low-frequency imaging (Figure 6). As suggested by the data in Figures 2 and 4, signal enhancement at a PI of 10 s increased progressively with MI ($p\leq0.01$ for linear trends) for both agents. However, for both high- and low-frequency imaging, intensity at an MI of 0.1 was lower for Sonazoid than for Definity, implying a threshold effect for producing strong non-linear signal from Sonazoid requiring an MI >0.1.

Characterization of Cavitation

The amplitude-frequency histograms obtained by PCD for the two microbubble agents during at 1.8 MHz ultrasound are shown in Figure 7. At an MI of 0.1 there was slightly greater non-linear signal from stable cavitation from Definity than Sonazoid illustrated by a slightly greater second harmonic response. Strong non-linear signal from stable cavitation

was found at an MI ≥0.2 for both agents, indicated by higher second harmonic peaks than at MI 0.1. However, at MIs of 0.2 and higher, Definity underwent much more inertial cavitation indicated by the large elevation in broad band signal between the harmonic peaks. These spectral data profiles are consistent with greater acoustic lability for Definity than Sonazoid at MI of 0.2 and higher.

Canine Limb Perfusion Imaging

Real-time CEU perfusion imaging of the canine hindlimb using low-frequency ultrasound and destruction-replenishment algorithms was performed at an MI of 0.1 to 0.3. Real-time imaging was performed using a frame rate of 2 Hz (PI of 0.5 s). This imaging rate was selected based on the data in Figure 3 because it minimizes inter-pulse destruction and yet it provides a sufficient number of frames to reconstruct accurate replenishment curves after a high-MI pulse sequence. At an MI of 0.1, signal enhancement was low for both agents but was greater for Definity than Sonazoid (Figure 8, illustrative images in Supplemental Figure C). With sequential increase in MI, there was a progressive increase in signal enhancement for Sonazoid whereas signal for Definity stayed relatively constant. For quantitative analysis, the mean A-value for Definity did not significantly vary with increasing MI (15.9±4.5, 13.1±6.6, and 11.8±1.5 IU; ANOVA p=0.41); whereas it increased sequentially for Sonazoid (9.9±2.4, 53.5±24.5, 55.8±10.3 IU; ANOVA p=0.004). These data indicate the ability to generate robust post-destructive time-intensity data in limb skeletal muscle when using intermediate MI (0.2 to 0.3) with Sonazoid microbubbles. Of note, microvascular flux rate (β) increased slightly when increasing the MI from 0.2 to 0.3 for both Definity (0.13±0.6 vs 0.37±0.14 s^{-1}, p=0.02) and to a lesser extent with Sonazoid (0.11±0.6 vs 0.26±0.13 s^{-1}, p=0.07) consistent with previous findings that show that occult microbubble destruction between imaging frames produces an artificial shortening of β.[15]

Murine limb perfusion imaging which was performed only with Sonazoid indicated that signal intensity achieved during high-power intermittent imaging was significantly but only mildly higher than that achieved during intermediate-power real-time imaging (Supplemental Figure D). Since there is little destruction of Sonazoid when imaged at 7 MHz and MI up to 0.4, there was no significant differences in the average β-values at the different MIs.

DISCUSSION

In this study, we investigated a new imaging strategy designed to produce robust limb skeletal muscle perfusion data during real-time CEU imaging that was leveraged on differences in the viscoelastic properties of lipid-shelled microbubble agents. We tested whether CEU signal enhancement could be amplified compared to standard real-time imaging by using intermediate-rather than low-power imaging together with a microbubble agent that has been observed to be particularly resilient during ultrasound exposure.[9] During high or low-frequency contrast-specific imaging, Sonazoid microbubbles were found to produce strong non-linear signal from stable cavitation at an MI ≥0.2 but with much less destruction from inertial cavitation than Definity. As a result, Sonazoid coupled with

intermediate power imaging provided strong signal enhancement during real-time CEU limb perfusion imaging.

In the evaluation of patients with PAD, there is currently no non-invasive imaging method that is routinely used to measure limb muscle perfusion at rest or perfusion abnormalities during stress. Traditional radionuclide approaches that have been used for decades for myocardial stress-rest imaging have not been applied largely because of the need for quantitative assessment rather than regional heterogeneity of perfusion. Quantitative methods such CEU,[1,2] magnetic resonance imaging (gadolinium-enhanced and arterial spin labeling),[16,17] and quantitative radionuclide imaging[18] have shown promise for assessing perfusion deficits in PAD. CEU is an attractive approach because of practical considerations of cost, speed, and the preexisting presence of ultrasound in vascular laboratories. Limb CEU has been used extensively to study endogenous and therapeutic angiogenesis in pre-clinical models.[11,19,20] In humans, however, CEU like MRI is plagued by weak signal enhancement when using conventional FDA-approved microbubble doses owing to the low blood flow in skeletal muscle at rest (0.05 to 0.2 ml/min/g).[4,5] As a result, destruction-replenishment algorithms have had to be performed with intermittent high-MI imaging which is difficult to perform.

The rationale up to now for using intermittent high-MI imaging to assess limb perfusion in patients with PAD is that signal from microbubbles exposed to ultrasound around their resonant frequency increases with the MI.[21] As the acoustic pressure is increased, there is an increase in stable non-linear cavitation and eventually inertial cavitation which produces strong broad-band signals.[22] The inertial cavitation during high-power intermittent CEU perfusion imaging not only produces strong signal, but is also used to plot replenishment curves when time is incrementally increased between destructive pulses.[13,14] On the other hand, real-time perfusion imaging relies on non-linear signals that must be generated by imaging pulses that produce little microbubble destruction. Hence, real-time myocardial contrast echocardiography is rarely performed at an MI of 0.2 or above. For limb imaging, the MI at which microbubble destruction occurs is lower than myocardium because of absence of the chest wall has a high attenuation coefficient (>1 dB/cm/MHz).[23]

In this study, we first evaluated whether Sonazoid microbubbles are more resistant to inertial cavitation than Definity. Both PCD and CEU imaging with clinical scanners showed this to be the case. Despite the greater acoustic durability and lower compressibility of Sonazoid on bulk modulus measurement, they produced an equal amount of signal enhancement in vivo as Definity at an MI ≥0.2 when measurements were made at long PIs which negate the effect of destruction. As a result, during intermediate-power CEU perfusion imaging in the canine limb, Sonazoid delivered at clinically-relevant doses produced robust post-destruction time-intensity curves. With Definity, signal at shorter PIs decreases due to intertial cavitation. Hence, during real-time perfusion imaging, signal did not increase with sequential increase of MI to the intermediate range (0.2–0.3) due to the offset of microbubble destruction by each frame (2 Hz).

The more robust signal enhancement with Sonazoid with incremental increase in the MI would not be expected to alter quantitative perfusion data since plateau signal enhancement

is normalized to blood pool signal which also increases. However, increasing the MI also resulted in a trend toward higher β-values, although less so for Sonazoid than Definity. The reason for this finding has been modeled and well described during in vivo imaging, and is due to a subtle increase in the replenishment rate constant when microbubbles are destroyed between each pulse.[15] For this reason, during high-frequency murine real-time imaging where there is no destruction even at MI=0.4, the β-value did not differ for a wide range of acoustic pressures. The implication of these findings is that the eventual translation to humans must be performed with the knowledge that subtle microbubble destruction must be excluded in order to not overestimate β.

Although differences in acoustic durability could be attributable to differences in the density of the gas cores for Sonazoid (C_4F_{12}) and Definity (C_3F_{10}), a more likely explanation resides in differences in shell characteristics.[21,24] Several different models of non-linear oscillation for “soft-shelled” microbubbles have been derived from the parent Rayleigh-Plesset model of bubble acoustic behavior. In these models, viscous damping is a critical factor in determining bubble stability and the magnitude and type of oscillation.[21,25] Shell elasticity, coating viscosity, shell friction, surface tension, and the ability to undergo “shell buckling” during compression phase have all been proposed to influence viscous damping.[21,25,26] These factors are in large part determined by the lipid constituents of the shell which differ substantially for Definity and Sonazoid. It should be noted that bubble size also influences surface tension so that the greater proportion of small microbubbles (<2 μm) for Definity may have contributed to its destruction at lower pressures.

The very low signal generation for Sonazoid at an MI of 0.1 which then “catches up” to Definity at higher MIs is consistent with the notion of pressure thresholding where microbubble vibration will only begin after a certain acoustic pressure is applied.[27] This phenomenon may be due in part to changes in elastic properties of encapsulated microbubbles when the surface lipid concentration changes during forced oscillation, referred to by some as “strain softening”.[27,28]

The potential clinical impact of our findings is substantial. For destruction-replenishment perfusion imaging algorithms, the ability to use real-time imaging makes it possible to assess perfusion in seconds rather than minutes. High-MI intermittent perfusion imaging is quite challenging in the leg since it is difficult to maintain a steady imaging plane at the relatively long PI required to reach plateau intensity in PAD patients (15 to 20 seconds), and because stress-rest imaging requires exercise which puts the muscle in motion. Real-time CEU imaging would not only simplify image acquisition, but could also make bilateral and multi-level perfusion imaging more readily achievable. Irrespective of the approach for assessing perfusion (destruction-replenishment or bolus transit rate analysis), high signal-to-noise is of critical importance when evaluating patients with critical limb ischemia in whom resting perfusion can be very low. It is worth noting that intermediate MI imaging with acoustically-resilient microbubbles may improve the quality of myocardial perfusion imaging as well since low-MI cardiac imaging is often fraught with a narrow balance between non-linear signal generation and destruction.

There are several limitations of the study that deserve attention. Not all results are directly applicable to humans since skeletal muscle blood flow is substantially greater in mice than in humans, which is why we opted to also study a canine model with low-frequency imaging. We also did not quantify absolute microvascular blood volume in these studies which would have allowed CEU assessment of absolute blood flow. We studied only two different contrast-specific multi-pulse imaging techniques. These techniques were chosen based on the recognition that they are among the most sensitive for microbubble signal detection in patients. With regard to the hydrophone measurements, the peak negative acoustic pressures measured with the 7 MHz probe were lower than one would predict based on the displayed MI. This discrepancy was apparently a result of near-field imaging for the transducer since pressures measured 4–5 mm farther from the transducer increased substantially (40%, 35%, 40% and 30% for MI of 0.1, 0.2, 0,3 and 0.4; respectively). Finally, we limited our evaluation to only two ultrasound contrast agents, although in vitro studies indicate that Sonazoid is also substantially more stable than Optison when ultrasound is applied at similar frequencies.[9]

In summary, we have demonstrated that a new imaging regime that employs intermediate acoustic pressures, acoustically durable microbubbles, and slow frame-rate continuous imaging can substantially improve the ability to generate robust limb perfusion imaging data. This advance may be an important step towards adoption of CEU in clinical practice or for its use for measuring effect of new therapies in patients with PAD. Human studies will need to be performed to confirm these findings.

Supplementary Material

Refer to Web version on PubMed Central for supplementary material.

Acknowledgments

FUNDING SOURCES

Dr. Seol is supported by a grant from the Inje Research and Scholarship Foundation. Dr. Davidson is supported by a Clinical Research Program Award (12CRP11890055) from the American Heart Association. Dr. Lindner is supported by grants R01-HL078610 and R01HL111969 from the National Institutes of Health.

REFERENCES

1. Lindner JR, Womack L, Barrett EJ, Weltman J, Price W, Harthun NL, et al. Limb stressrest perfusion imaging with contrast ultrasound for the assessment of peripheral arterial disease severity. JACC Cardiovasc Imaging. 2008;1:343–50 [PubMed: 19356447]
2. Duerschmied D, Olson L, Olschewski M, Rossknecht A, Freund G, Bode C, et al. Contrast ultrasound perfusion imaging of lower extremities in peripheral arterial disease: A novel diagnostic method. Eur Heart J. 2006;27:310–5 [PubMed: 16308326]
3. Duerschmied D, Zhou Q, Rink E, Harder D, Freund G, Olschewski M, et al. Simplified contrast ultrasound accurately reveals muscle perfusion deficits and reflects collateralization in pad. Atherosclerosis. 2009;202:505–12 [PubMed: 18606414]
4. Bonadonna RC, Saccomani MP, Del Prato S, Bonora E, DeFronzo RA, Cobelli C. Role of tissue-specific blood flow and tissue recruitment in insulin-mediated glucose uptake of human skeletal muscle. Circulation. 1998;98:234–41 [PubMed: 9697823]

5. Heinonen I, Kemppainen J, Kaskinoro K, Peltonen JE, Borra R, Lindroos MM, et al. Comparison of exogenous adenosine and voluntary exercise on human skeletal muscle perfusion and perfusion heterogeneity. J Appl Physiol (1985). 2010;108:378–86 [PubMed: 19940098]
6. Womack L, Peters D, Barrett EJ, Kaul S, Price W, Lindner JR. Abnormal skeletal muscle capillary recruitment during exercise in patients with type 2 diabetes mellitus and microvascular complications. J Am Coll Cardiol. 2009;53:2175–83 [PubMed: 19497445]
7. Duerschmied D, Maletzki P, Freund G, Olschewski M, Bode C, Hehrlein C. Success of arterial revascularization determined by contrast ultrasound muscle perfusion imaging. J Vasc Surg. 2010;52:1531–6 [PubMed: 20843628]
8. Chin CT, Burns PN. Predicting the acoustic response of a microbubble population for contrast imaging in medical ultrasound. Ultrasound Med Biol. 2000;26:1293–300 [PubMed: 11120367]
9. Moran CM, Anderson T, Pye SD, Sboros V, McDicken WN. Quantification of microbubble destruction of three fluorocarbon-filled ultrasonic contrast agents. Ultrasound Med Biol. 2000;26:629–39 [PubMed: 10856626]
10. de Jong N, Hoff L, Skotland T, Bom N. Absorption and scatter of encapsulated gas filled microspheres: Theoretical considerations and some measurements. Ultrasonics. 1992;30:95–103 [PubMed: 1557838]
11. Carr CL, Qi Y, Davidson B, Chadderdon S, Jayaweera AR, Belcik JT, et al. Dysregulated selectin expression and monocyte recruitment during ischemia-related vascular remodeling in diabetes mellitus. Arterioscler Thromb Vasc Biol. 2011;31:2526–33 [PubMed: 21885854]
12. Bragadeesh T, Sari I, Pascotto M, Micari A, Kaul S, Lindner JR. Detection of peripheral vascular stenosis by assessing skeletal muscle flow reserve. J Am Coll Cardiol. 2005;45:780–5 [PubMed: 15734625]
13. Dawson D, Vincent MA, Barrett EJ, Kaul S, Clark A, Leong-Poi H, et al. Vascular recruitment in skeletal muscle during exercise and hyperinsulinemia assessed by contrast ultrasound. Am J Physiol Endocrinol Metab. 2002;282:E714–20 [PubMed: 11832377]
14. Wei K, Jayaweera AR, Firoozan S, Linka A, Skyba DM, Kaul S. Quantification of myocardial blood flow with ultrasound-induced destruction of microbubbles administered as a constant venous infusion. Circulation. 1998;97:473–83 [PubMed: 9490243]
15. Leong-Poi H, Swales J, Jayaweera AR, Bin JP, Kaul S, Lindner JR. Effect of microbubble exposure to ultrasound on quantitation of myocardial perfusion. Echocardiography. 2005;22:503–9 [PubMed: 15966935]
16. Pollak AW, Meyer CH, Epstein FH, Jiji RS, Hunter JR, Dimaria JM, et al. Arterial spin labeling mr imaging reproducibly measures peak-exercise calf muscle perfusion: A study in patients with peripheral arterial disease and healthy volunteers. JACC Cardiovasc Imaging. 2012;5:1224–30 [PubMed: 23236972]
17. Isbell DC, Epstein FH, Zhong X, DiMaria JM, Berr SS, Meyer CH, et al. Calf muscle perfusion at peak exercise in peripheral arterial disease: Measurement by first-pass contrast-enhanced magnetic resonance imaging. Journal of magnetic resonance imaging : JMRI. 2007;25:1013–20 [PubMed: 17410566]
18. Stacy MR, Yu da Y, Maxfield MW, Jaba IM, Jozwik BP, Zhuang ZW, et al. Multimodality imaging approach for serial assessment of regional changes in lower extremity arteriogenesis and tissue perfusion in a porcine model of peripheral arterial disease. Circ Cardiovasc Imaging. 2014;7:92–9 [PubMed: 24170237]
19. Ryu JC, Davidson BP, Xie A, Qi Y, Zha D, Belcik JT, et al. Molecular imaging of the paracrine proangiogenic effects of progenitor cell therapy in limb ischemia. Circulation. 2013;127:710–9 [PubMed: 23307829]
20. Leong-Poi H, Christiansen J, Heppner P, Lewis CW, Klibanov AL, Kaul S, et al. Assessment of endogenous and therapeutic arteriogenesis by contrast ultrasound molecular imaging of integrin expression. Circulation. 2005;111:3248–54 [PubMed: 15956135]
21. Sarkar K, Shi WT, Chatterjee D, Forsberg F. Characterization of ultrasound contrast microbubbles using in vitro experiments and viscous and viscoelastic interface models for encapsulation. The Journal of the Acoustical Society of America. 2005;118:539–50 [PubMed: 16119373]

22. Church CC, Carstensen EL. “Stable” inertial cavitation. Ultrasound Med Biol. 2001;27:1435–7 [PubMed: 11731057]

23. Teotico GA, Miller RJ, Frizzell LA, Zachary JF, O’Brien WD, Jr. Attenuation coefficient estimates of mouse and rat chest wall. IEEE Trans Ultrason Ferroelectr Freq Control. 2001;48:593–601 [PubMed: 11370373]

24. Borden MA, Kruse DE, Caskey CF, Zhao S, Dayton PA, Ferrara KW. Influence of lipid shell physicochemical properties on ultrasound-induced microbubble destruction. IEEE Trans Ultrason Ferroelectr Freq Control. 2005;52:1992–2002 [PubMed: 16422411]

25. Marmottant P, van der Meer S, Emmer M, Versluis M, de jong N, Hilgenfeldt S, et al. A model for large amplitude oscillations of coated bubbles accounting for buckling and rupture. The Journal of the Acoustical Society of America. 2005;118:3499–505

26. Overvelde M, Garbin V, Sijl J, Dollet B, de Jong N, Lohse D, et al. Nonlinear shell behavior of phospholipid-coated microbubbles. Ultrasound Med Biol. 2010;36:2080–92 [PubMed: 21030140]

27. Emmer M, van Wamel A, Goertz DE, de Jong N. The onset of microbubble vibration. Ultrasound Med Biol. 2007;33:941–9 [PubMed: 17451868]

28. Tsiglifis K, Pelekasis NA. Nonlinear radial oscillations of encapsulated microbubbles subject to ultrasound: The effect of membrane constitutive law. The Journal of the Acoustical Society of America. 2008;123:4059–70 [PubMed: 18537358]

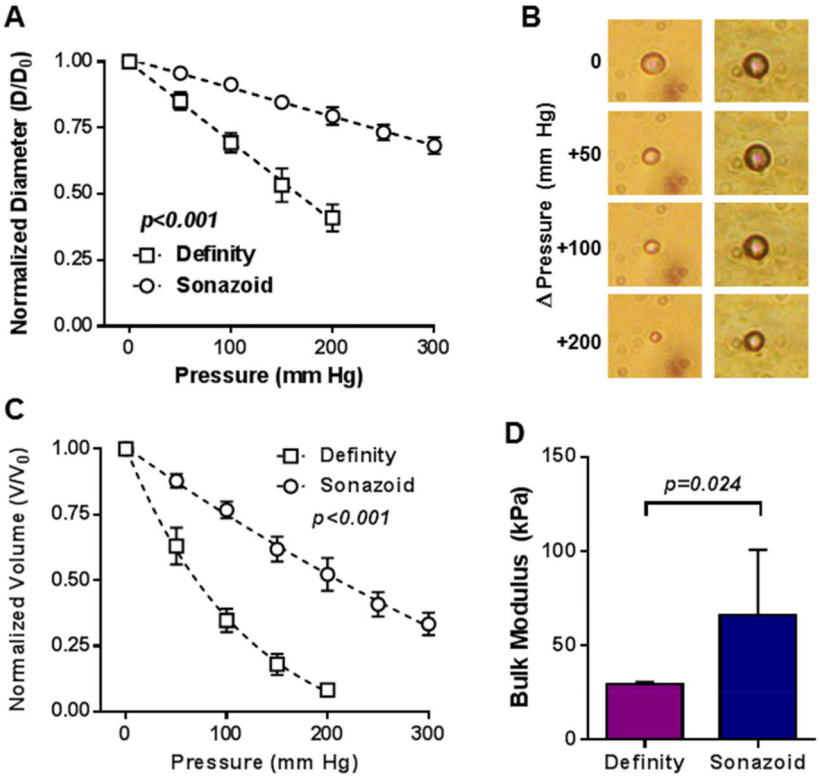

Figure 1.

(A) Mean (±SEM) microbubble diameter with sequential increases in pressure from ambient atmospheric pressure (0 mm Hg). (**B**) Representative microscopy images of Definity (left) and Sonazoid (right) microbubbles with incremental increases in ambient pressure. (**C**) Mean (±SEM) microbubble volume with sequential increases in pressure from ambient atmospheric pressure (0 mm Hg). (**F**) Mean (±SEM) bulk modulus measured using a 200 mm Hg pressure increase. ANCOVA P-values for panels A and C reflect differences in the slope of linear regression for diameter and rate constant of exponential decay for volume.

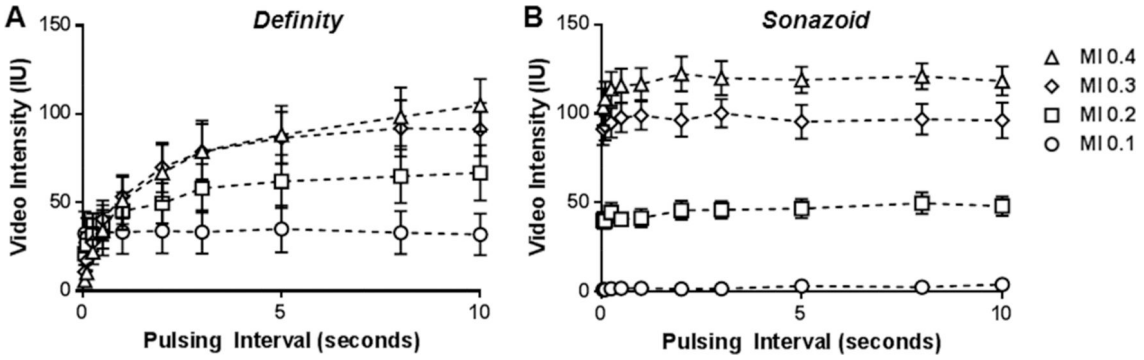

Figure 2.

Mean (±SEM) video intensity values during high-frequency CEU of the the murine hindlimb performed at various pulsing intervals and mechanic indices (MI) for (**A**) Definity and (**B**) Sonazoid.

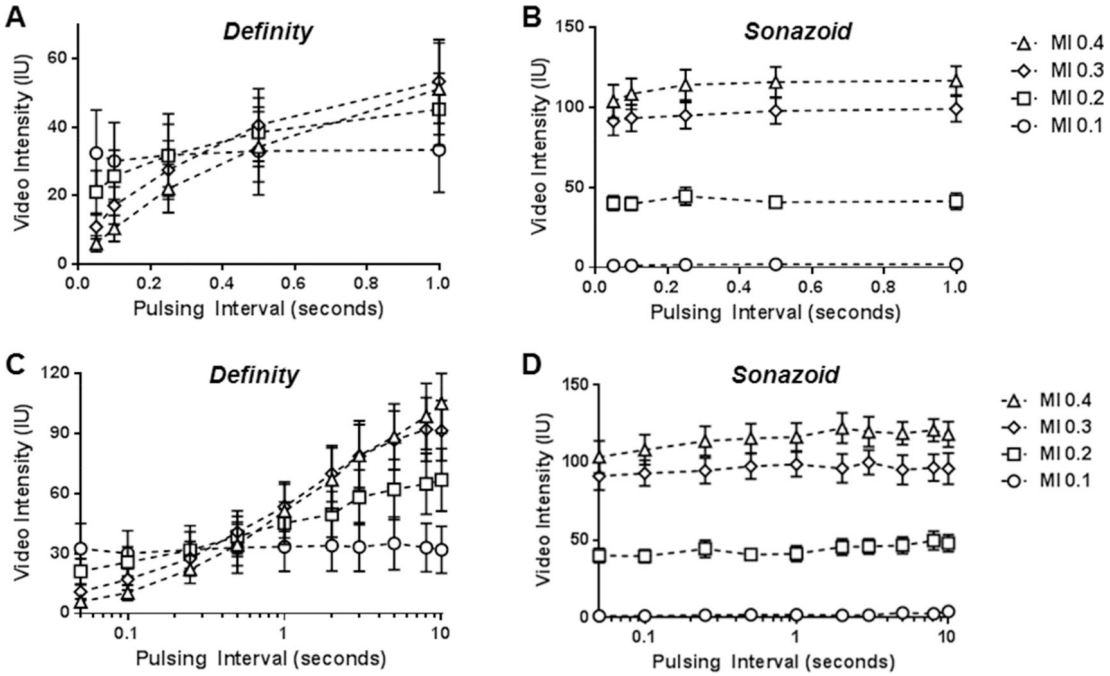

Figure 3.

Mean (±SEM) video intensity values during high-frequency CEU of the the murine hindlimb similar to those in Figure 2 but displayed either with an abbreviated pulsing interval scale ending at 1.0 second (**A** and **B**), or with full pulsing interval range displayed on a log-compressed scale (**C** and **D**) in order to appreciate differences at short pulsing intervals.

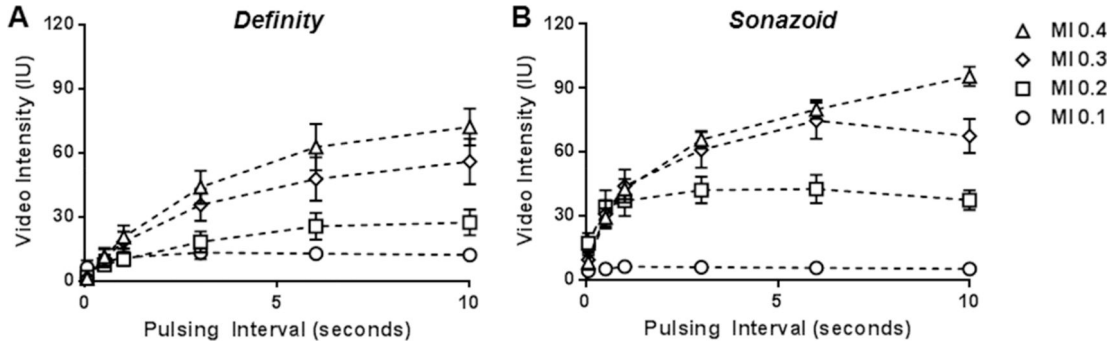

Figure 4.

Mean (±SEM) video intensity values during low-frequency CEU of the the canine hindlimb performed at various pulsing intervals and mechanic indices (MI) for (**A**) Definity and (**B**) Sonazoid.

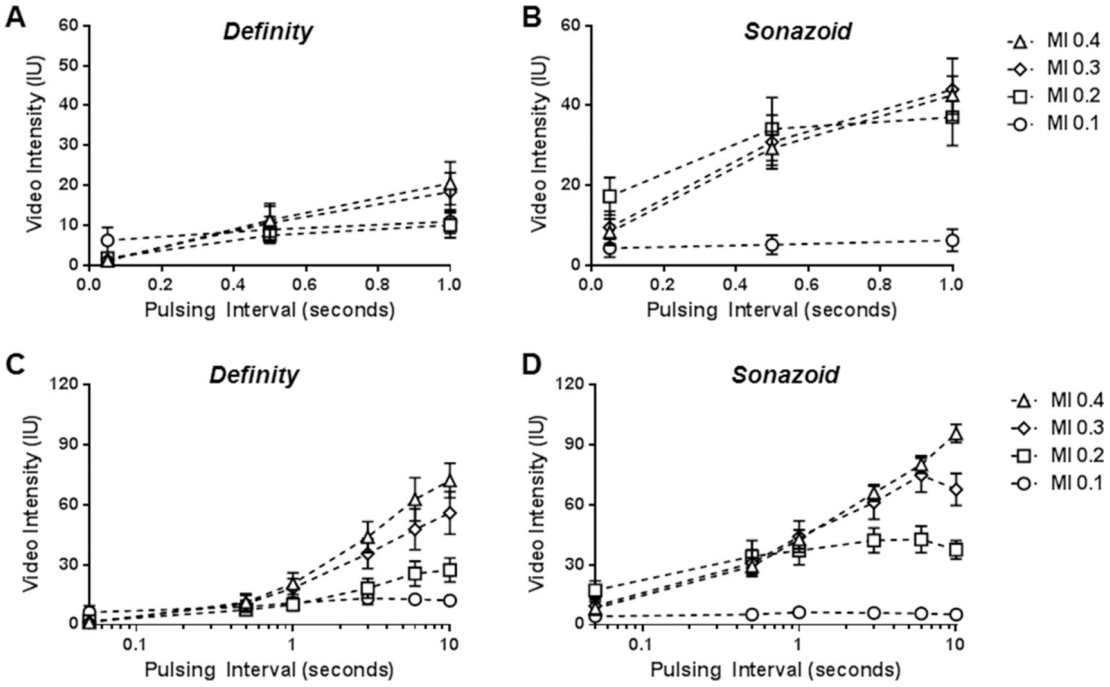

Figure 5.

Mean (±SEM) video intensity values during low-frequency CEU of the the canine hindlimb similar to those in Figure 4 but displayed either with an abbreviated pulsing interval scale ending at 1.0 second (**A** and **B**), or with full pulsing interval range displayed on a log-compressed scale (**C** and **D**) in order to appreciate differences at short pulsing intervals.

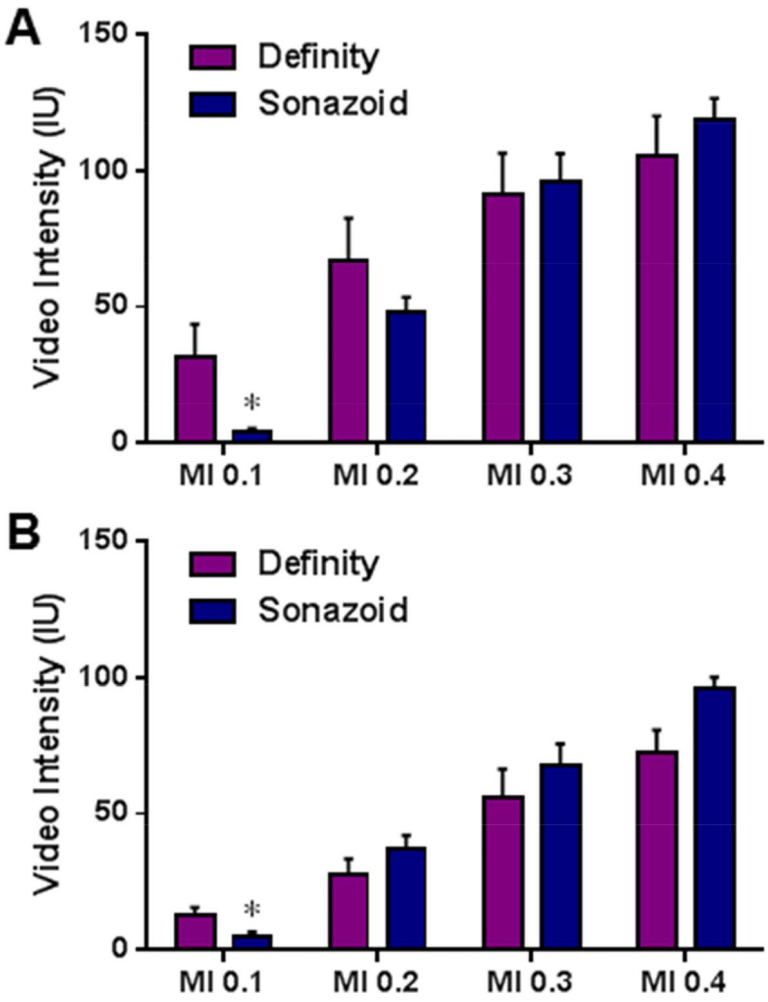

Figure 6.

Mean (±SEM) video intensity values obtained at the longest pulsing interval (10 s) for each mechanical index (MI) during (**A**) high-frequency CEU in the murine hindlimb, and (**B**) low-frequency CEU imaging in the canine hindlimb. *p<0.05 versus Definity. For both agents, test for linear trends for an increase in intensity with MI were p<0.01 for the murine model and p=0.01 for the canine model.

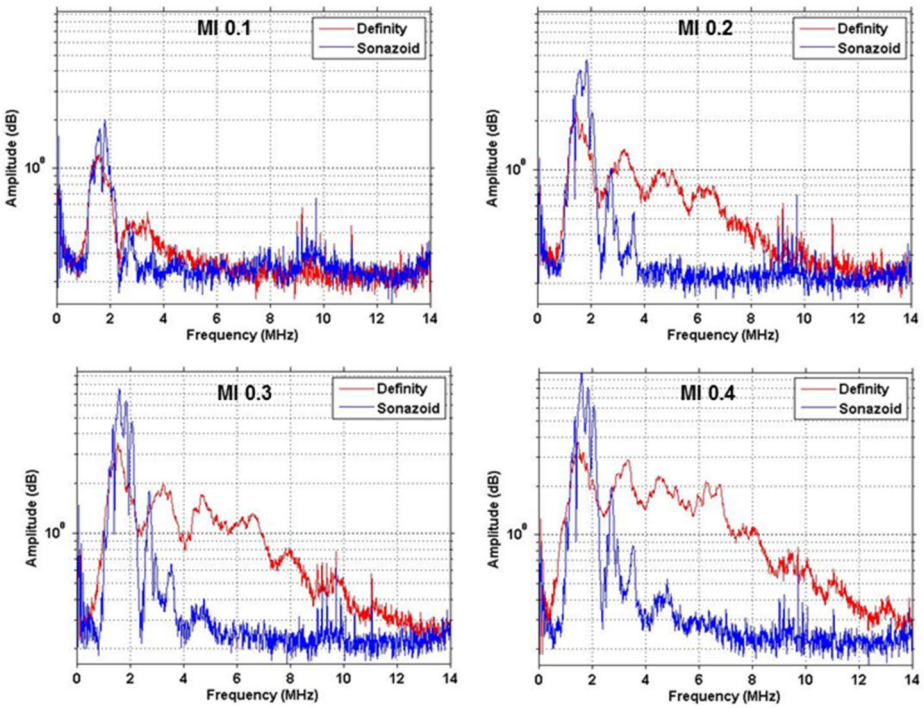

Figure 7.

Amplitude-frequency histograms for Definity (red) and Sonazoid (blue) obtained during ultrasound imaging at 1.8 MHz illustrating greater degree of broad-band signal (inertial cavitation) for Definity at MI 0.2 and greater. Harmonic peaks, illustrating stable cavitation, are seen for both agents at all powers.

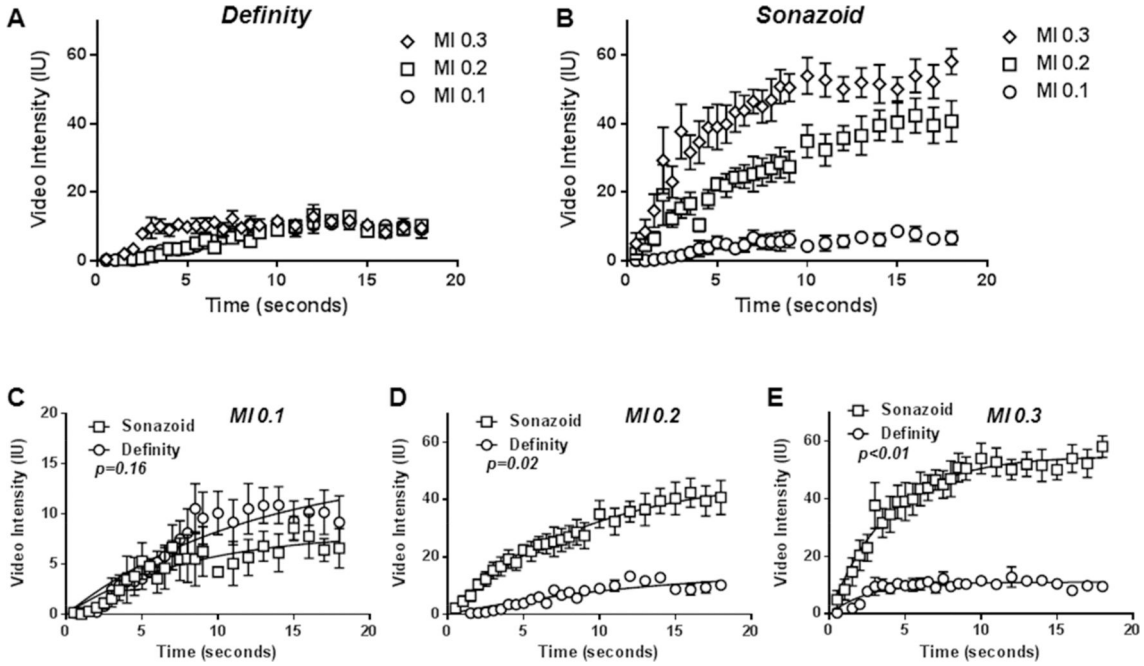

Figure 8.

Mean (±SEM) video intensity values obtained during real-time CEU perfusion imaging in the canine hindlimb obtained at a frame rate of 2 Hz (PI 0.5 s) after a high-power destructive pulse sequence for (**A**) Definity and (**B**) Sonazoid. Differences in A-values are provided in the text. (**C** to **D**) CEU perfusion data redisplayed according to mechanical index (MI) to illustrate differences between agents. P-values are presented for differences in the A-values.

TABLE 1.

Peak Negative Acoustic Pressure (kPa) Measured at the Ultrasound Focal Depth*

	Transducer Frequency	
Mechanical Index	**1.8 MHz**	**7 MHz†**
0.1	130 kPa	120 kPa
0.2	270 kPa	290 kPa
0.3	400 kPa	470 kPa
0.4	510 kPa	600 kPa

* pressures are rounded to the nearest 10 kPa

† pressures at this frequency are lower than predicted due to near-field imaging (see Discussion).